CO$_2$ Adsorption Capacity of Activated N-Doping Porous Carbons Prepared from Graphite Nanofibers/Polypyrrole

Long-Yue Meng,[1,2] Wan Meng,[2] Tie Chen,[1,3] Long Yi Jin[1,3]

[1]Key Laboratory of Natural Resources of Changbai Mountain and Functional Molecules, Yanbian University, Yanji 133002, China
[2]Department of Chemical Engineering, Yanbian University, Yanji 133002, China
[3]Department of Chemistry, Yanbian University, Yanji 133002, China
Correspondence to: L. Y. Jin (E-mail: lyjin@ybu.edu.cn)

ABSTRACT: In this study, N-doping porous carbons (NPCs) with a 3D aperiodic hierarchical and layered structure were prepared by the sodium hydride (NaOH) activation of graphite nanofibers (GNFs)/polypyrrole (PPY) composites. The effects of the N groups and structural features on the CO$_2$ adsorption capacity of NPCs were investigated by N$_2$ full isotherms, XRD, SEM, and TEM. The CO$_2$ adsorption capacity was measured by the CO$_2$ isothermal adsorption at 25°C and 1 atm. It was found that GNFs served as a substrate and layered graphitic carbons were formed by the thermal annealing of PPY. The content of N groups and textural properties of NPCs were enhanced with increasing activation temperature, resulting in improved CO$_2$ adsorption capacity. The CO$_2$ adsorption isotherms showed that GPK-600 exhibited the best CO$_2$ adsorption capacity of 88.8 mg/g when the activation temperature was 600°C. The result indicates that the pore size and its distribution of NPCs lead to feasible contact CO$_2$, and the presence of high N groups on the NPCs could have resulted in further stabilization of the surface effect. © 2014 Wiley Periodicals, Inc. J. Appl. Polym. Sci. **2014**, *131*, 40517.

INTRODUCTION

CO$_2$ emissions are damaging to the environment and the earth. Since the industrial revolution, human activities have led to the emission of large quantities of greenhouse gases owing to the effects of industrialization worldwide. Global CO$_2$ emissions are causing climate change and related environmental problems. To avoid irreversible and adverse effects to the climate, sustainable empowerment should be adopted through the advancement of science and technology in the field of carbon capture, utilization, and storage. This involves the use of established technologies to capture, transport, and utilize or store CO$_2$ emissions from large point sources such as power stations.[1]

Capturing CO$_2$ is probably most effective at point sources such as large fossil fuel or biomass energy facilities, industries with high CO$_2$ emissions, natural gas processing, synthetic fuel plants, and fossil-fuel-based hydrogen production plants.[1] Numerous capture technologies have been developed for capturing CO$_2$ from flue gas, such as CO$_2$ absorption, adsorption, membrane separation, and chemical looping combustion.[2–5]

Therefore, it is necessary to improve CO$_2$ adsorption technologies for achieving low energy consumption.

Porous materials for efficient CO$_2$ capture should not only fit the attributes of a CO$_2$ molecule (kinetic size and polarizability) but also satisfy the requirements of the CO$_2$ capture process (dynamics, operation, etc.)[5] Thus far, various porous CO$_2$ capture materials such as carbon zeolites, metal-organic frameworks (MOFs), silica, and polymers have been used.[6–11] Porous carbons play an important role in CO$_2$ capture owing to their highly porosity, extended surface area, surface chemistry, and thermal stability.[5–7,11,12] Recently, N-doping porous carbons (NPCs) possessing well-defined micro-/mesopores and N-containing groups have attracted much attention.[13,14] Several studies have examined a simpler route for the preparation of NPCs, which have been extensively investigated as CO$_2$ adsorbents owing to their excellent basic organic group/inorganic metal oxide and high porosity.[15–17] Furthermore, NPCs always contain a large number of pores (∼2 nm), and they exhibit better CO$_2$ adsorption performance than mesoporous network materials.

Graphite nanofibers (GNFs) are one of the most promising carbon nanomaterials for many applications such as catalytic support, polymer reinforcement agents, electrodes, and gas adsorbents. In many cases, the problem associated with these structures is that their porosity is not very good (specific surface area of ~200 m^2/g), a situation that is detrimental for many applications such as those involving gas adsorption. Chemical activation with a metal hydride, such as KOH or NaOH, is the most common process utilized to introduce pores in bulk carbon and carbon fibers. Different methods such as cutting, cap-opening, or chemical treatment have been used to increase the specific surface area of carbon nanotubes (CNTs) and carbon nanofibers (CNFs). In this regard, the porosity of GNFs can be significantly modified by chemical activation processes that remove the most reactive carbon atoms from their structure, leading to both an increase in the specific surface area and formation of an abundant network of both micropores and mesopores. In a previous study, Meng and Park developed highly porous GNFs by a KOH activation method for CO_2 adsorption.[6] They reported that the specific surface area of GNFs increased from 178 to 567 m^2/g. However, the high CO_2 adsorption capacity in exfoliated GNFs could not be reproduced, and it is difficult for the GNFs to adsorb a large amount of CO_2 merely by weak physical adsorption. Currently, N doping has been considered a feasible approach to tune the physical and chemical properties of carbon materials owing to the presence of additional lone pairs of electrons in the N atom as compared with the carbon atom.[13] Many studies have reported on the preparation of N-doped CNFs/CNTs; however, few studies have reported on the preparation of N-doped and high-porosity GNFs for CO_2 adsorption.

With this in mind, in this study, we have prepared NPCs using a GNFs/polypyrrole (PPY) blend as a precursor and NaOH as an activating agent. PPY was selected as both a carbon source and an N source owing to its very high nitrogen content. Enriched N together with micro-/mesopores was successfully introduced into the resultant carbons. The combination of a chemical activation approach and polymer blending strategy leads to resultant carbons that can be used as materials with high CO_2 adsorption capacity.

MATERIALS AND METHODS

Materials and Methods

The GNFs (straight type, length: 25–30 μm) were treated with HNO$_3$/H$_2$SO$_4$ (Analytical reagent, Tianjin Boda) mixture solutions. Totally, 1 g of oxidized GNFs was dispersed in 100 mL of 0.5M of FeCl$_3$ (FeCl$_3$ · 6H$_2$O, Sigma-Aldrich) solution with stirring for 1 h. The mixture was maintained at 5°C. Finally, 0.3M of distilled pyrrole (Reagent grade, 98% Sigma-Aldrich) was added to the above solution for 30 min to initiate polymerization.[18] The GNFs/PPY composites were then washed using water and methanol. The washed powder was dried in a vacuum oven at 80°C for 24 h.

The GNFs/PPY composites were activated chemically by heating GNFs/PPY composites and an NaOH (Analytical reagent, Tianjin Boda Co.) mixture (GNFs/PPY composites, PPY at a weight ratio of 3) to 600–900°C (heating rate: 5°C min^{-1}, holding
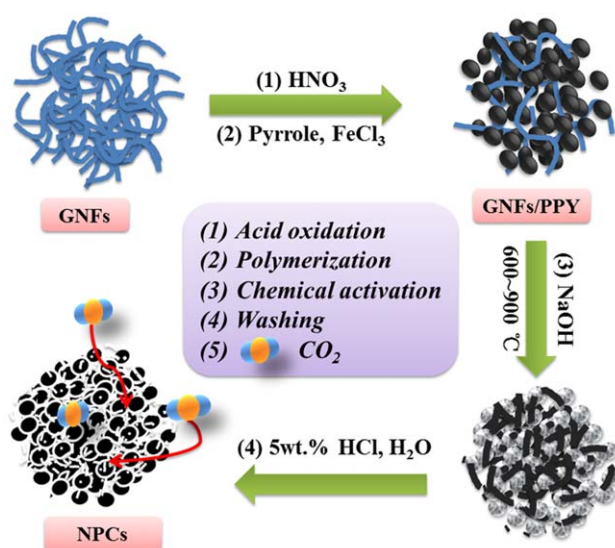

Figure 1. Preparation procedure of the NPCs. [Color figure can be viewed in the online issue, which is available at wileyonlinelibrary.com.]

time: 2 h) under N$_2$. The activated samples were then washed several times with HCl (10 wt %) to remove any inorganic salts and then washed with distilled water until a neutral pH was attained. Finally, the activated carbons were dried in an oven at 80°C. The chemically activated carbons were denoted as GPK-600, GPK-700, GPK-800, GPK-850, and GPK-900. Figure 1 shows a schematic diagram of the steps involved in NPC formation using an NaOH activation method.

Characterization

Wide-angle X-ray diffraction (XRD) patterns of the samples were obtained using a Rigaku Model D/MAX-III B diffractometer equipped with a rotation anode that used CuK_α radiation (λ = 0.15418 nm). Diffraction patterns were recorded for a 2θ range of 10–60°. A scanning electron microscope (SEM, Hitachi/S-4200) and field-emission transmission electron microscope (FE-TEM, JEM2100F/JEOL) were used to characterize the morphology of the NPCs. The specific surface area and total pore volume were determined by physically adsorbing N$_2$/77 K using a surface area analyzer (BEL, Japan). The N$_2$ adsorbed on the NPCs was used to calculate the specific surface area using the BET (Brunauer-Emmett-Teller) equation. The total pore volume was estimated to be the liquid volume of nitrogen at a relative pressure of ~0.995, and the micro- and mesopore structures were analyzed by using the D-R (Dubinin−Radushkevich) and BJH (Barrett-Joyner-Halenda) equations, respectively. The CO_2 adsorption capacity was measured by the CO_2 isothermal adsorption at 25°C and 1 atm. Furthermore, the parameters of the D-A (Dubinin–Astakhov) equation were obtained from CO_2 adsorption.

RESULTS AND DISCUSSION

The average (002) interlayer spacing (d_{002}) and the average stacking height of graphitic carbon (002) planes of GNFs, as prepared GNFs/PPY composites, and activated NPCs in this study were analyzed by powdered X-ray diffraction, as shown in Figure 2. It was found that the peaks could be explained in
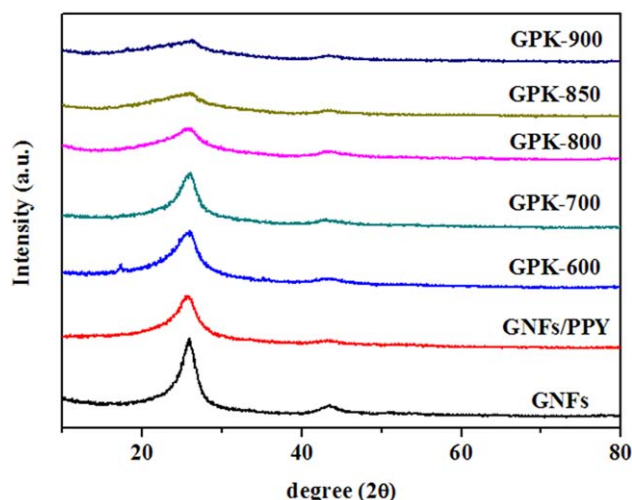
Figure 2. XRD patterns of the pristine GNFs, GNFs/PPY composites, and NPCs. [Color figure can be viewed in the online issue, which is available at wileyonlinelibrary.com.]

terms of the known structure of the graphitic carbon of GNFs at $2\theta = 26°$ (002) and 43.5° (100). The results showed that the average stacking height of graphitic carbon peaks decreased with an increase in the activation temperature owing to the increase in the disorder of the layer structures and the decrease in the crystalline size via the NaOH activation process. For the same reason, the highest values for graphitic carbon peaks (d_{002}) were obtained when NaOH was used as the activating agent because the strongest interaction occurred in this case.[6] Furthermore, a decrease in the highest of graphitic carbon peaks (d_{002}) intensity indicates that an increase in the irregularity of layer structures and a widening of the peak range have resulted in collapse-like layer structures. This is because a higher activation temperature causes broadening and collapsing of the overall (d_{002}) plane interspacing to break down and rearrange the fibrous structure.[19]

The textural parameters of the pristine GNFs and prepared NPCs were confirmed by typical N_2/77 K adsorption/desorption measurements. The shapes of the N_2/77 K full isotherm curve and hysteresis can be used to study the size distribution, shape, and structure of the pore inside porous materials. All the isotherms are of IV isotherms according to IUPAC classification, and they show a hysteresis loop at relative pressures above 0.4, indicating the presence of mesopores in all the samples (Figure 3). The result suggests that samples produced at higher activation temperature are composed mainly of micro-/mesopores. The comparison of the curves of all samples shows that NaOH activation promotes the development of micro-/mesoporosity in the samples through the etching of the GNFs/PPY composites at different temperatures. The adsorption capacity increased significantly with the activation temperature. The changes in the shape of the isotherms with increasing activation temperature from 600 to 900°C indicate the changes in the pore structure of the prepared NPCs. The shape of the isotherms for GPK-600 changed between types I and IV isotherms with an abrupt bend at low relative pressures, P/P_o, followed by a slight

increase in N_2 adsorption at high relative pressures. This suggests that samples produced at low activation temperature are composed mainly of micropores (GPK-600), and that the materials synthesized at high activation temperature are composed mainly of micro-/mesopores (GPK-700, GPK-800, GPK-850, and GPK-900).

The specific surface area, micropore volume, mesopore volume, total pore volume, micropore pore volume ratio, and average pore diameter for a series of samples are summarized in Table I for comparison. The prepared materials possess very high specific surface area, large pore volumes, and smaller pore diameters. The specific surface area and total pore volume of NPCs increased significantly with increasing activation temperature from 785 m²/g (600°C) to 1222 m²/g (850°C) and from 0.400 cm³/g (600°C) to 0.934 cm³/g (900°C), respectively, which is larger than that of pristine GNFs (126 m²/g, 0.190 cm³/g) and GNFs/PPY composites (11 m²/g, 0.043 cm³/g). It can be seen that the increase in total pore volume is accompanied by an increase in the micro-/mesopore volumes. It was also observed that the micropore volumes were mainly enhanced in the GPK-800 samples. However, it was interesting to note that the micropore fractions of the NPCs decreased with increasing activation temperature. Micropore development at lower temperature (600°C) can indeed result from the etching of PPY. After heat treatment, the average pore size of NPCs decreases up to GPK-850, but then increases for GPK-900. This is because NaOH activation has generally been attributed to the partial blockage of the microporous system by the decomposed products generated during the activation process. With regard to mesopore development at higher temperature, GNFs are ascribed to the partial gasification and expansion of the interlayer spacing between graphenes through simultaneous intercalation and deintercalation.[6,19]

Figure 4 shows the pore size distributions of the pristine GNFs and NPCs. As shown in Figure 4(a), the prepared NPCs exhibit a narrow micropore size distribution centered around 6.5 Å.
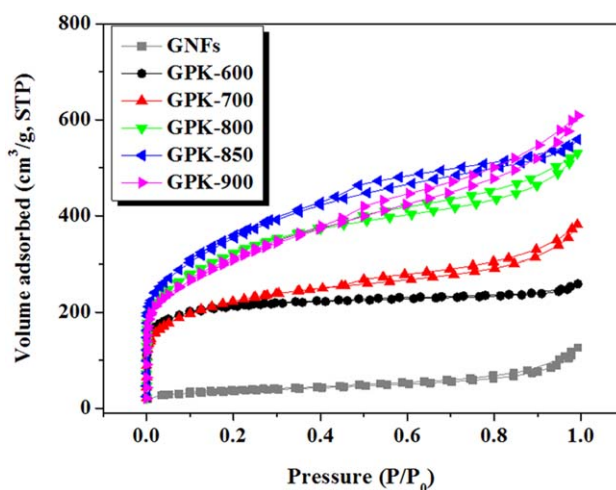

Figure 3. The N_2/77 K full isotherms of the pristine GNFs and NPCs. [Color figure can be viewed in the online issue, which is available at wileyonlinelibrary.com.]

Table I. Pore Structure Parameters for the Pristine GNFs, GNFs/PPY Composites, and N-Enriched Porous Carbons

Samples	S_{BET}[a] (m^2/g)	V_{Mi}[b] (cm^3/g)	V_{Me}[c] (cm^3/g)	V_T[d] (cm^3/g)	F_M[e] (%)	AD[f] (Å)
GNFs	126	0.024	0.166	0.190	12.6	60.1
GNFs/PPY	11	0.001	0.042	0.043	2.4	80.1
GPK-600	785	0.270	0.130	0.400	67.5	20.3
GPK-700	781	0.208	0.379	0.587	35.4	30.1
GPK-800	1136	0.254	0.563	0.817	31.1	28.8
GPK-850	1222	0.252	0.609	0.861	29.3	28.2
GPK-900	1107	0.205	0.729	0.934	21.9	33.7

[a] Specific surface area (m^2/g): BET equation ($p/p_0 = 0.05$-0.1).
[b] Micropore volume (cm^3/g): Dubinin–Radushkevich equation.
[c] Mesopore vbolume (cm^3/g): BJH equations.
[d] Total pore volume (cm^3/g): V_{ads} ($P/P_0 = 0.995$) $\times 0.001547$.
[e] Fraction of micropore (%).
[f] Average pore diameter (Å): $2 \times S_{BET}/V_{ads}$.

The pore diameter of the NPCs can apparently be finely controlled simply by using the NaOH activation method to prepare NPCs with different micropore diameters. As shown in Figure 4(b), the prepared NPCs mainly consist of mesopores of less than 300 Å in diameter. After NaOH activation, in the treated GNFs, narrow mesopore development can be observed around the region of pore radii of 17–63 Å, where the mesopore size tends to be lesser than 200 Å. Among the samples prepared, GPK-850 exhibits superior textural parameters including high specific surface area, large pore volume, and the smallest pore diameter that could allow the NaOH activation temperature to favor the formation of micropores, whereas temperatures in excess of 900°C favored the formation of mesopores. Extensive gasification causes a breakthrough in the micropore walls, resulting in an increase in the mesopore volumes.[20–22]

Figure 5 shows SEM and TEM images of the pristine GNFs, GNFs/PPY composites, and NPCs. The GNFs/PPY composites were used as a carbon precursor, and they exhibited an unregular granular morphology. The prepared NPCs exhibited a range of shapes depending on the degree of activation [Figure 5(b–f)].

The prepared NPCs consisted of short GNFs and large macroporous carbons. In this study, the pristine GNFs have a diameter of approximately 100–200 nm. After PPY polymerization and the activation of the GNFs/PPY composite by heat treatment, the morphologies of the prepared NPCs were not similar to those of the pristine GNFs and showed a decreased length compared with the pristine GNFs [Figure 5(a–f)]. After activation, the NPCs exhibited a fibrous structure with lengths ranging from 2 to 10 μm [Figure 5(f)]. The formation of the NPCs was further observed using TEM images. Comparisons of the contrast of the images show that the NPCs have a carbon-coated GNFs structure with high aspect ratio [Figure 5(h)]. Based on the above discussion, NaOH activation has a significant effect on the fiber morphology and pore size distribution inside NPCs owing to the escape of H, N, and O during carbonization.[23]

Table II lists the chemical composition of the prepared NPCs. The N content decreased with increasing activation temperature. As a result, N is oxidized and removed more easily than carbon during the activation process. This reduction was particularly
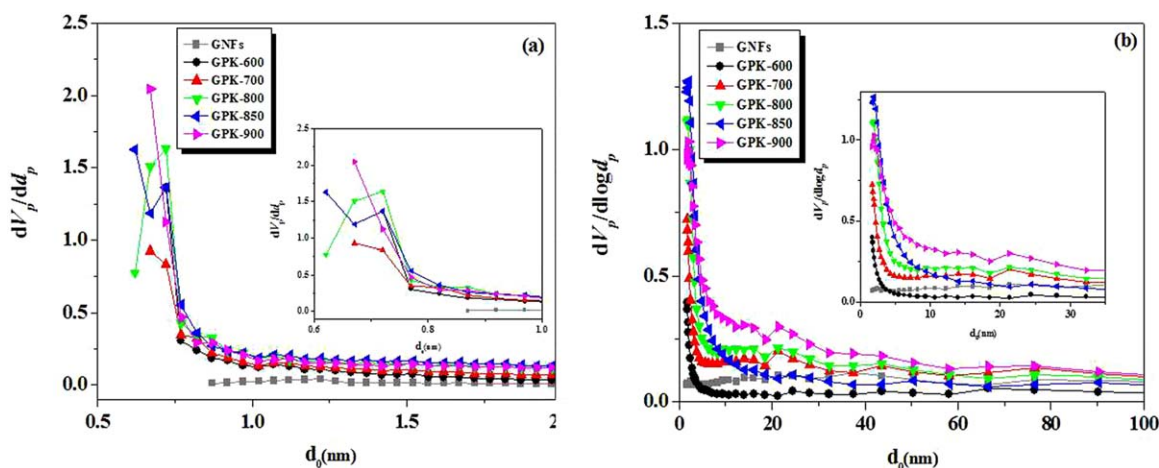

Figure 4. Pore size distributions of the pristine GNFs and NPCs: (a) micropore size distributions, (b) mesopore size distribution. [Color figure can be viewed in the online issue, which is available at wileyonlinelibrary.com.]
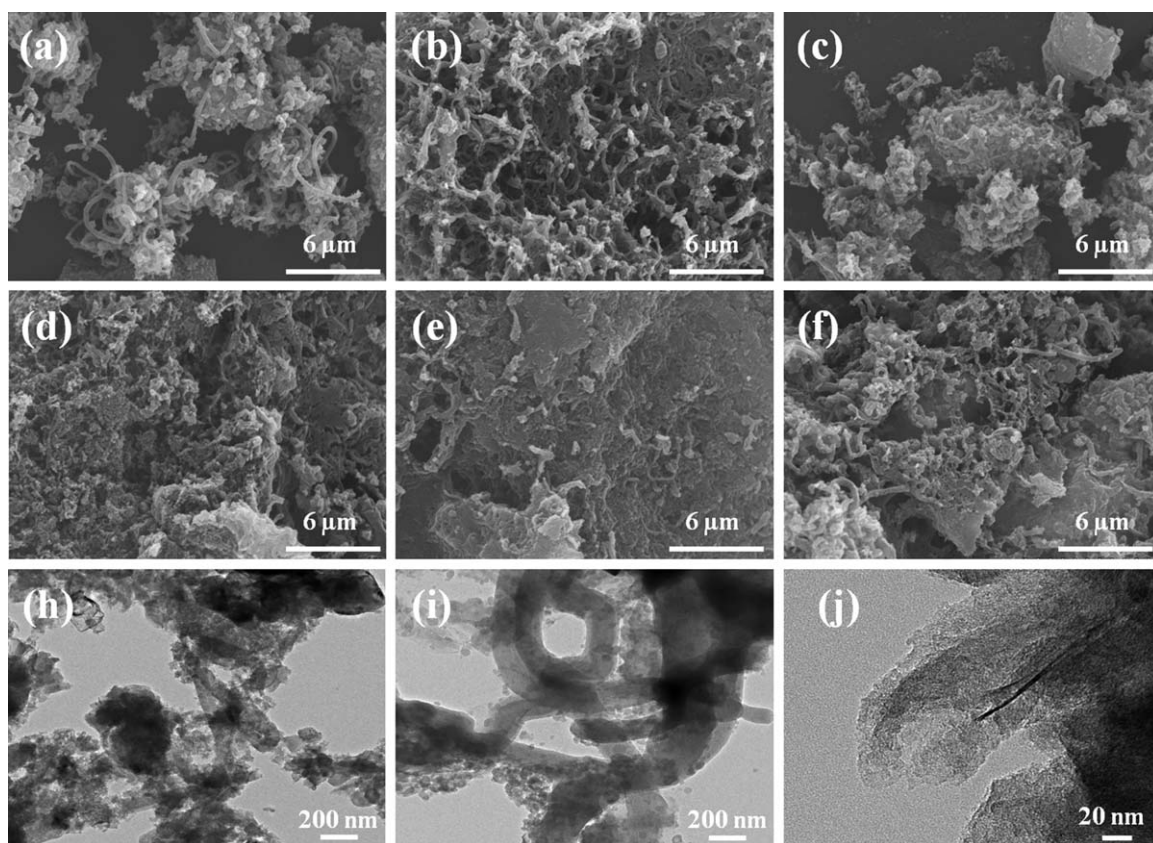
Figure 5. SEM (a–f) and TEM (h–j) image of GNFs/PPY composites, and NPCs: (a) GNFs/PPY, (b) GPK-600, (c) GPK-700, (d) GPK-800, (e) GPK-850, (f) GPK-900, and (h–j) GPK-800.

drastic from 600 to 700°C. Remarkably, the GPK-600 sample contained a very large amount of N (6.64 wt %), which is one of the largest N contents ever reported for highly N-doping porous carbons. The 399.7 eV peak corresponds to pyridinic-N of the GNFs/PPY sample and the 398.1 and 400.7 eV peaks correspond to pyrrolic-/pyridonic-N of GPK-600.[25] Although pyridinic-N and quaternary-N are more stable N species under pyrolytic conditions, pyridonic-N groups are more likely to be formed under oxidizing conditions such as those present during chemical activation.[25,26] The high N content of the samples activated under mild conditions combined with the fact that N forms pyridonic-N structures might be beneficial for CO_2 capture because these basic N species can act as an anchor for CO_2 capture.[25–27]

Table II also shows the textural parameters calculated from the CO_2 adsorption isotherms at 25°C. As shown in Table II, in the case of GPK-600, the specific surface area and total pore volume are higher than those in the case of others. Figure 7 shows the pore size distributions of the pristine GNFs and the prepared NPCs from CO_2/298 K isotherms. As shown in Figure 7(a), the micropore structures were predominantly enhanced by NaOH activation, whereas the distributions show that a slight development can be observed around the narrow microregion (∼6.2 Å). As shown in Figure 7(b), the pore distributions of NPCs show that narrow mesopore development can be observed around the region of pore radii of ∼20 Å, where the size of the

mesopore tends to be lesser than 100 Å. Lower temperatures (600°C) favored the formation of narrow micropores and mesopores.

Figure 8 shows CO_2 excess sorption isotherms obtained at 298 K for all samples. For all studied NPCs, the isotherm behavior is of Type I (as defined by the IUPAC classification), which characterizes the microporous adsorbent (monolayer
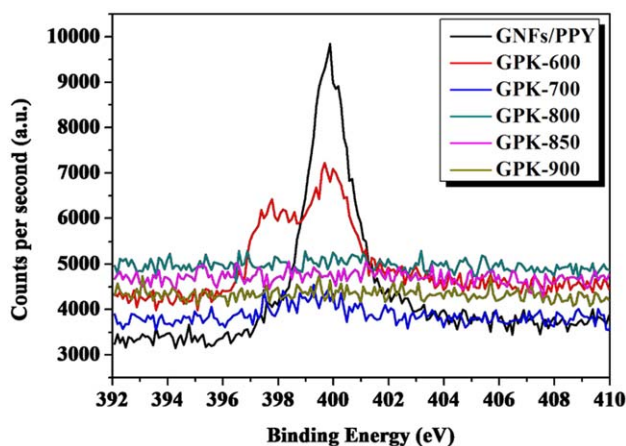

Figure 6. N1s XPS spectra for the GNFs/PPY and NPCs. [Color figure can be viewed in the online issue, which is available at wileyonlinelibrary.com.]

Table II. Chemical Composition and Pore Structure Parameters from CO_2 Adsorption Isotherms of the Prepared NPCs (wt %)

Samples	Chemical composition (wt %)			Textural properties		
	C	O	N	S_{BET}[a]	V_T[b]	D[c]
GNFs/PPY	74.21	16.47	9.32	32	0.023	28.2
GPK-600	83.82	9.55	6.64	112	0.081	29.0
GPK-700	81.43	17.17	1.4	83	0.057	27.5
GPK-800	90.57	8.76	0.67	106	0.076	28.5
GPK-850	87.59	11.04	1.37	104	0.078	29.8
GPK-900	85.96	13.48	0.56	87	0.064	29.2

[a] Specific surface area (m^2/g): BET equation ($p/p_0 = 0.05$–0.1).
[b] Total pore volume (cm^3/g): V_{ads} ($P/P_0 = 0.995$) $\times 0.001547$.
[c] Average pore diameter (Å): $2 \times S_{BET}/V_{ads}$.

adsorption). According to previous studies, the activation of carbon materials with NaOH or KOH can lead to a change in the pore size distribution.[6,20–24] The researchers reported that the mechanism of NaOH is similar to that of KOH and that the same high surface area activated carbon could be obtained using both NaOH and KOH activation. The molecular weight of KOH (56.1 g/mol) is larger than that of NaOH (40.0 g/mol). Thus, the dosage (weight measurement) of NaOH-activated carbon is less than that of KOH-activated carbon.[20] NaOH is cheaper and less corrosive than KOH, and it is more environmentally friendly based on lifecycle assessment.

Recent researches demonstrated that high specific surface area and total pore volume are not the decisive factors for high CO_2 adsorption capacity, and the narrow micropores less than 1 nm and incorporate heteroatoms such as N are more effective in CO_2 adsorption. Because of CO_2 adsorption performance diminishes quickly with an increasing temperature, and large-scale application of that technology requires an integral biowaste recovery system.[28] As shown in Figure 8, the activated GNFs/PPY composites showed better performance for CO_2 adsorption than the pristine GNFs. The high CO_2 adsorption capacity and extent of microporosity can be further increased by NaOH activation. This clearly indicates that chemical activa-

tion by NaOH increases the affinity of GNFs toward CO_2. It can also be seen that the adsorbed weights (CO_2) of all of the GNFs are in the following order at a low relative pressure range ($P/P_0 < 0.4$): GPK-600 > GPK-800 > GPK-850 > GPK-700 > GPK-900 > GNFs. However, they are in the following order in the region of middle and high relative pressures ($P/P_0 \geq 04$): GPK-600 > GPK-850 > GPK-800 > GPK-900 > GPK-700 > GNFs. Other hand, the above XPS analysis reveals that basic heteroatom N are generated after carbonization and activation, which being served as basic sites to improve the affinity of the carbon surface to CO_2. The increase in narrow micropore volume and increased total basicity (N doping concentration) of the NPCs is the result of the increase in CO_2 adsorption capacity that occurs during activation at 600°C. The mechanisms of N increasing the CO_2 adsorption capacity and selectivity include base–acid interaction, quadrupolar interaction, and hydrogen bonds.[28–31]

To develop a CO_2 adsorbent with high adsorption capacity, its pore distribution and surface chemistry must both be considered. Han et al. have prepared a series of N-doped carbons with very high N doping concentration (ca., 13%) and large surface area of 890 m^2/g (arising from micropores, <1 nm) by a nanocasting route using tri-continuous mesoporous silica IBN-9 as a
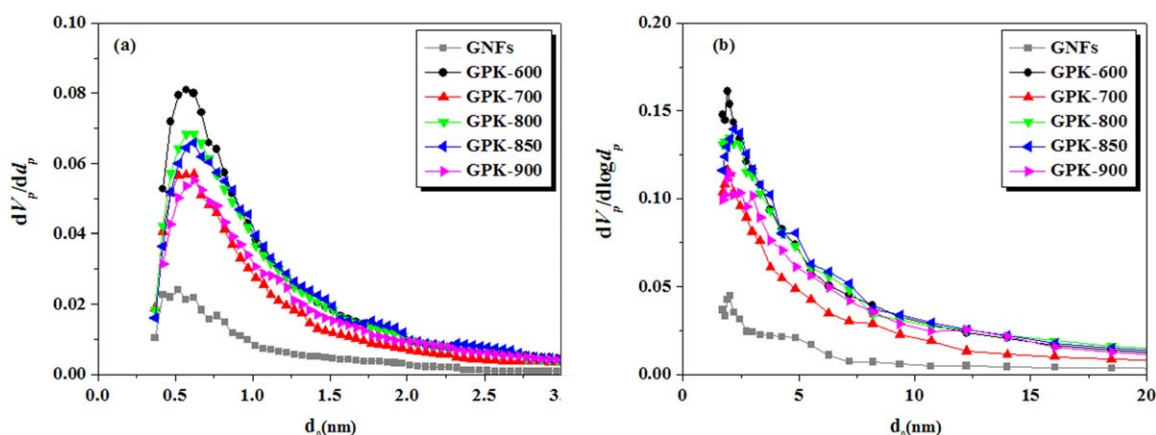

Figure 7. Pore size distributions of the pristine GNFs and NPCs from CO_2 adsorption: (a) micropore size distributions, (b) mesopore size distribution. [Color figure can be viewed in the online issue, which is available at wileyonlinelibrary.com.]
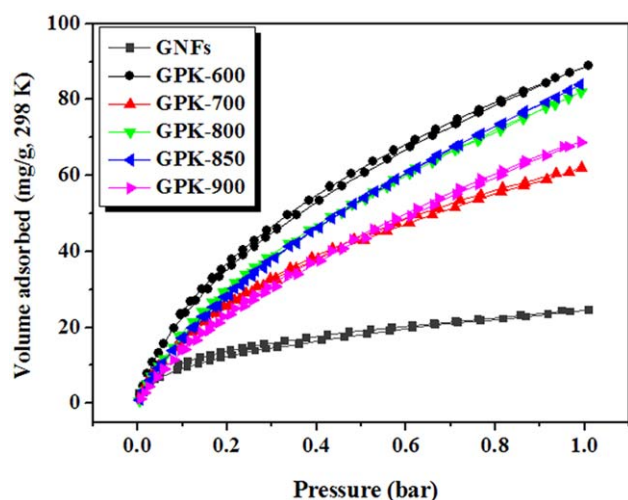
Figure 8. The CO_2/298 K adsorption/desorption isotherms of the pristine GNFs and NPCs. [Color figure can be viewed in the online issue, which is available at wileyonlinelibrary.com.]

hard template. These are highly desirable characteristics for selective CO_2 capture (4.50 mmol/g, 298 K, and 1 bar).[32] In our previous studies, the pristine GNFs were enhanced by a chemical activation process that involved an activation temperature of 900°C at a fixed KOH ratio (GNFs:KOH = 1:3.5), which showed the best CO_2 adsorption capacity of 59.2 mg/g at 298 K and 1 bar.[6] The results of this study showed that the adsorption capacity of GPK-600 was higher than the value reported by Meng and Park (ca., 59.2 mg/g) under similar conditions.[6]

In addition to the CO_2 capture technology, CO_2 selectivity is an important parameter because practical applications are always associated with mixtures of different gases such as N_2, CH_4, H_2, etc.[33,34] Pure porous carbons with high specific surface area (e.g., activated carbons, CNTs, mesoporous carbons) have high CO_2 adsorption capacity but show low CO_2/N_2 selectivity.[35]

Compared with pure porous carbons, the incorporation of N-doping carbons can selectively improve the CO_2 adsorption capacity over N_2 or other gases. Figure 9 shows the N_2 adsorption isotherms of GPK-600 at 298 K. Apparently, the samples have a much higher adsorption capacity for CO_2 than for N_2. It should be noted that the high N contents (9.32%) and narrow micropore distribution give rise to significantly enhanced CO_2/ N_2 selectivity; this, combined with the high adsorption capacities, makes the prepared NPCs promising CO_2 adsorbents for selective CO_2 capture form power plant flue gas.

In addition, the CO_2 adsorption capacities of various porous carbons materials including commercial activated carbons (CACs, S_{BET} = 1211 m^2/g, V_{micro} = 0.048 cm^3/g, V_{total} = 1.382 cm^3/g, and $D_{diammer}$ = 3.8 nm), graphite nanofibers (GNFs, S_{BET} = 178 m^2/g, V_{micro} = 0.060 cm^3/g, V_{total} = 0.250 cm^3/g, and $D_{diammer}$ = 5.7 nm), mesoporous carbons (MC, S_{BET} = 575 m^2/g, V_{micro} = 0.030 cm^3/g, V_{total} = 0.543 cm^3/g, and $D_{diammer}$ = 4.8 nm), multiwalled carbon nanotubes (MWCNTs, S_{BET} = 209 m^2/g, V_{micro} = 0.030 cm^3/g, V_{total} = 0.610 cm^3/g, and $D_{diammer}$ = 11.7 nm), grapheme nanoplatelets (GNPs, S_{BET} = 480 m^2/g, V_{micro} = 0.001 cm^3/g, V_{total} = 1.730 cm^3/g, and $D_{diammer}$ = 14.4 nm), and GPK-600 have been tested for comparison.

Figure 9(b) shows the CO_2 adsorption isotherms of these porous materials. Commercial activated carbons (CACs), graphite nanofibers (GNFs), mesoporous carbons (MC), multiwalled carbon nanotubes (MWCNTs), and grapheme nanoplatelets (GNPs) exhibit the maximum CO_2 adsorption capacities at 81.2 mg/g, 24.5 mg/g, 81.2 mg/g, 48.0 mg/g, 11.2 mg/g, and 79.5 mg/g, respectively. The advantage of the larger narrow micropore and N groups in GPK-600 becomes more evident as the pressure is increased, leading to the higher CO_2 capture capacity of GPK-600 as compared with that of five carbon materials under the same conditions (Pressure = 1 bar). All these results suggest that the large CO_2 adsorption capacities of the NPCs are due to a combination of both narrow microporosity and a large number of basic N functional groups.
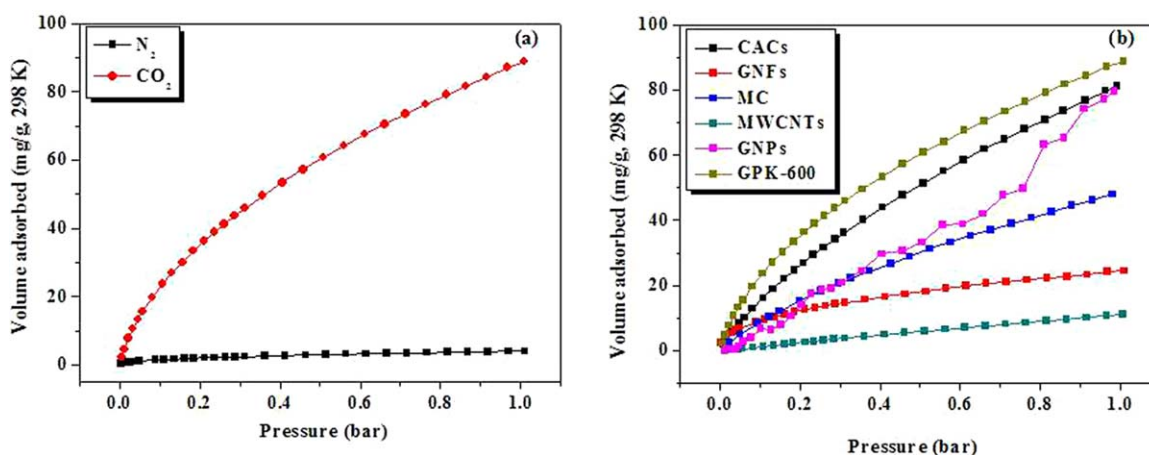

Figure 9. (a) The CO_2 and N_2 adsorption isotherms of NPCs at 298 K (GPK-600); (b) CO_2 adsorption isotherms of commercial activated carbons (CACs), graphite nanofibers (GNFs), mesoporous carbons (MC), multi-walled carbon nanotubes (MWCNTs), grapheme nanoplatelets (GNPs), and GPK-600 measured at 1bar and 298 K. [Color figure can be viewed in the online issue, which is available at wileyonlinelibrary.com.]

CONCLUSIONS

A series of NPCs with a 3D aperiodic hierarchical and layered structure have been prepared using GNFs/PPY composites as a carbon source and NaOH as an activation agent. Additional narrow microporosity was generated in these NPCs through a mild chemical activation temperature. The use of PPY carbon precursors allows the integration of high N content and large narrow micropore distribution in the prepared NPCs. The N groups and textural properties of NPCs increased with increasing activation temperature, resulting in enhanced CO_2 adsorption capacity. The CO_2 adsorption isotherms showed that GPK-600 exhibited the best CO_2 adsorption capacity of 88.8 mg/g when the activation temperature was 600°C. The result indicates that the pore size and its distribution of NPCs lead to feasible contact CO_2, and the presence of high N groups on the NPCs could have resulted in further stabilization of the surface effect. GPK-600 has a higher N content and high micropore volume, and it shows even higher CO_2/N_2 selectivity under 298 K and 1 bar.

REFERENCES

1. Leimkühler, H. J. Managing CO Emissions in the Chemical Industry; Wiley: New York, **2010**; Chapter *11*, p 389.

2. Rochelle, G. T. *Science* **2009**, *25*, 1652.

3. Luis, P.; Bruggen, B. V. *Greenhouse Gas. Sci. Technol.* **2013**, *3*, 318.

4. MacDowell, N.; Florin, N.; Buchard, A.; Hallett, J.; Galindo, A.; Jackson, G. Adjiman, C. S.; Williams, C. K.; Shah, N.; Fennell, P. *Energy Environ. Sci.* **2010**, *3*, 1645.

5. Lu, A. H.; Hao, G. P. *Annu. Rep. Prog. Chem. Sect. A : Inorg. Chem.*, **2013**, *109*, 484.

6. Meng, L. Y.; Park, S. J. *J. Colloid Interface Sci.* **2010**, *352*, 498.

7. Meng, L. Y.; Park, S. J. *J. Colloid Interface Sci.* **2010**, *366*, 125.

8. Meng, L. Y.; Park, S. J. *J. Colloid Interface Sci.* **2012**, *386*, 285.

9. Bollini, P.; Didas, S. A.; Jones, C. W. *J. Mater. Chem.* **2011**, *285-290*, 15100.

10. Hedin, N.; Chen, L. J.; Laaksonen, A. *Nanoscale* **2010**, *2*, 1819.

11. Zhang, B.; Shi, Y.; Wu, Y.; Wang, T.; Qiu, J. *J. Appl. Polym. Sci.*, **2014**, *131*, 39925.

12. Wang, B.; Kong, Q.; Quan, F.; Ji, Q.; Xia, Y. *J. Appl. Polym. Sci.* **2013**, *128*, 2216.

13. Ma, C.; Shi, J.; Song, Y.; Zhang, D.; Zhai, X.; Zhong, M.; Guo, Q.; Liu, L. *Int. J. Electrochem. Sci.* **2012**, *7*, 7587.

14. Mane, G. P.; Dhawale, D. S.; Anand, C.; Ariga, K.; Ji, Q.; Wahab, M. A.; Mori, T.; Vinu, A. *J. Mater. Chem. A.* **2013**, *1*, 2913.

15. D'Alessandro, D. M.; Smit, B.; Long, J. R. *Angew. Chem. Int. Ed.* **2010**, *49*, 6058.

16. Xia, Y.; Makaya, R.; Grant, D. M.; Walker, G. S. *Carbon* **2011**, *49*, 844.

17. Deng, Q. F.; Liu, L.; Lin, X. Z.; Du, G.; Liu, Y.; Yuan, Z. Y. *Chem. Eng. J.* **2012**, *203*, 2913.

18. Sevilla, M.; Valle-Vigón, P.; Fuerte, A. B. *Adv. Funct. Mater.* **2011**, *21*, 2781.

19. Kim, B. J.; Lee, Y. S. Park, S. J. *J. Colloid Interface Sci.* **2007**, *306*, 454.

20. Tseng, R. L. *J. Hazard. Mater.* **2007**, *147*, 1020.

21. Sun, Y.; Yue, Q.; Gao, B.; Li, Q.; Huang, L.; Yao, F.; Xu, X. *J. Colloid Interface Sci.* **2012**, *368*, 521.

22. Tseng, R. L. *J. Colloid Interface Sci.* **2012**, *303*, 494.

23. Wu, F. C.; Tseng, R. L. *J. Hazard. Mater.* **2008**, *152*, 1256.

24. Raymundo-Piñero, E.; Azaïs, P.; Cacciaguerra, T.; Cazorla-Amorós, D.; Linares-Solano, A.; Béguin, F. *Carbon* **2005**, *43*, 786.

25. Chandra, V.; Yu, S. U.; Kim, S. H.; Yoon, Y.S.; Kim, D. Y.; Kwon, A. H.; Meyyappan, M.; Kim, K. S. *Chem. Commun.* **2012**, *48*, 735.

26. Arenillas, A.; Drage, T. C.; Smith, K.; Snape, C. E. *J. Anal. Appl. Pyrol.* **2005**, *74*, 298.

27. Gu, J. M.; Kim, W. S.; Hwang, Y. K.; Huh, S. *Carbon* **2013**, *56*, 208.

28. Liu, Z.; Du, Z.; Song, H.; Wang, C.; Subhan, F.; Xing, W.; Yan, Z. *J. Colloid Interface Sci.* **2014**, *416*, 124.

29. Wang, L.; Yang, R. T. *J. Phys. Chem. C.* **2012**, *116*, 1099.

30. Vaidhyanathan, R.; Iremonger, S. S.; Shimizu, G. K.; Boyd, P. G. Alavi, S.; Woo, T. K. *Science* **2010**, *330*, 650.

31. Xing, W.; Liu, C.; Zhou, Z.; Zhang, L.; Zhou, J.; Zhuo, S.; Yan, Z.; Gao, H.; Wang, G.; Qiao, S. Z. *Energy Environ. Sci.* **2012**, *5*, 7323.

32. Zhao, Y.; Zhao, L.; Yao, K. X.; Yang, Y.; Zhang, Q.; Han, Y. *J. Mater. Chem.* **2012**, *22*, 19726.

33. Drage, T. C.; Snape, C. E.; Stevens, L. A.; Wood, J.; Wang, J.; Cooper, A. I.; Dawson, R.; Guo, X.; Satterley, C.; Irons, R. *J. Mater. Chem.* **2012**, *22*, 2815.

34. Bae, Y. S.; Farha, O. K.; Hupp, J. T.; Snurr, R. Q. *J. Mater. Chem.* **2009**, *19*, 2131.